

Damage Diagnosis in Semiconductive Materials Using Electrical Impedance Measurements

Richard W. Ross¹

NASA Langley Research Center, Hampton, Virginia, 23681-2199

and

Yolanda L. Hinton²

Army Research Laboratory, Hampton, Virginia, 23681-2199

Recent aerospace industry trends have resulted in an increased demand for real-time, effective techniques for in-flight structural health monitoring. A promising technique for damage diagnosis uses electrical impedance measurements of semiconductive materials. By applying a small electrical current into a material specimen and measuring the corresponding voltages at various locations on the specimen, changes in the electrical characteristics due to the presence of damage can be assessed. An artificial neural network uses these changes in electrical properties to provide an inverse solution that estimates the location and magnitude of the damage. The advantage of the electrical impedance method over other damage diagnosis techniques is that it uses the material as the sensor. Simple voltage measurements can be used instead of discrete sensors, resulting in a reduction in weight and system complexity. This research effort extends previous work by employing finite element method models to improve accuracy of complex models with anisotropic conductivities and by enhancing the computational efficiency of the inverse techniques. The paper demonstrates a proof of concept of a damage diagnosis approach using electrical impedance methods and a neural network as an effective tool for in-flight diagnosis of structural damage to aircraft components.

Nomenclature

f	=	applied current per unit volume
j	=	current density (charge per unit time per unit area)
k	=	thermal conductivity
q	=	heat flux
σ	=	electrical conductivity
T	=	temperature
V	=	electrical potential

I. Introduction

RECENT aerospace industry trends such as condition-based maintenance (CBM), in which aircraft maintenance is scheduled based on the condition of the vehicle instead of occurring at fixed time intervals, have resulted in an increased demand for real-time, effective techniques for in-flight structural health monitoring and damage diagnosis. Many traditional structural health monitoring approaches use discrete sensors such as strain gages or piezoelectric transducers for detecting regions of damage, but these methods may impose a stiff weight penalty due to wiring requirements for power and sensing. Other methods use fiber optic sensors or wireless sensors to reduce or eliminate much of the wiring constraints, but at the expense of additional complexity. Wireless sensors require batteries, either as a primary energy source or for energy storage, which increase vehicle weight and introduce maintenance issues.

¹ Aerospace Engineer, Durability, Damage Tolerance, and Reliability Branch, Mail Stop 188E, AIAA Member.

² Mechanical Engineer, Vehicle Technology Directorate, Mail Stop 266.

Accurate and timely assessment of airframe damage is a critical element of aviation safety, but analytical methods for diagnosing damage are often too computationally intensive to be suitable for in-flight assessment of damage. Direct analytical solutions to damage diagnosis problems can require hours or days of computational time on computers suitable for meeting the weight and power constraints of today's aircraft. Non-analytical (data-driven) techniques offer a computationally efficient alternative to analytical methods when an analytical solution to the problem does not exist or is not feasible.

Even when an analytical solution exists, its inverse may not. Consider a simple mathematical function, such as the sine function, which can be applied to an independent variable, x , to compute the dependent variable, y . In this case, there exists an inverse function, \sin^{-1} , which can be applied to y and should yield the initial value: x . However, not all mathematical functions have inverses that can be obtained by direct computation, especially for relationships with many independent and dependent variables. In these cases, approximations must be used. Inverse approaches are effective for applications where exact analytical solutions are not known or are too complex to be practical.

One such application is the in-flight identification and characterization of structural damage in airframe components. Techniques such as the finite element method (FEM) provide a *forward* analytical solution to the computation of physical properties (such as strains, displacements, and thermoelectrical characteristics) given a known damage state. However, there are no analytical techniques for solving the *inverse* problem: estimating damage from physical properties. In such cases, inverse approaches are warranted.

While some inverse methods are too computationally intensive, artificial neural networks (ANN) can be an effective and efficient approach for solving inverse problems. As described later in this paper, neural networks are "trained" to estimate the desired outputs from a set of inputs, while minimizing overall error. Although the training process can be quite arduous and time-consuming, a fully trained network can be quite efficient at estimating solutions to inverse problems.

This paper presents an effective and computationally efficient electrical impedance measurement-based method for *in situ* detection and characterization of airframe damage that is applicable to electrically semiconductive materials. Such materials are often used to provide shielding from sources of electromagnetic interference (EMI). By applying a small electrical current into a material specimen and measuring the corresponding electrical parameters such as voltage and resistance at various locations on the specimen, changes in these electrical characteristics due to the presence of damage can be detected. An artificial neural network uses these changes in electrical properties to provide an inverse solution that predicts the location and magnitude of the damage. The advantage of the electrical impedance method over other damage diagnosis techniques is that it uses the specimen itself as the sensor, requiring only simple voltage measurements instead of using discrete sensors, reducing weight and system complexity.

This research paper introduces a damage diagnostic approach using electrical impedance measurements and presents relevant background material on previous work using this technique. Next, the damage diagnosis approach is presented using FEM models to estimate electrical properties based on known damage conditions. The paper describes how the neural network uses these electrical property estimates to compute the inverse relationship: estimating damage characteristics from electrical properties. Next, the paper describes the testing and experimental demonstration of proof of concept for the damage diagnosis methodology. The paper concludes with a presentation of the results of this research effort.

II. Background

The concept of using the electrical properties of a material to assess damage originates with biomedical applications of Electrical Impedance Tomography (EIT) by Guardo, et al.¹ This technique was adapted to damage diagnosis of conductive plates by Morabito,² and later to composite beams and plates by Todoroki and Tanaka.³ These applications of EIT are based on changes in electrical resistance of semiconductive materials in response to the presence of structural damage.

Anderson, Lemoine, Ambur, and Love used boundary element method (BEM) models to generate electrical resistance predictions for training an artificial neural network to determine an inverse solution to the damage diagnosis problem.^{4,5} This approach used electrodes to apply small currents (50 mA, nominal) at known locations around the perimeter of specimens made from various semiconductive materials. These included conductive elastomers from Parker Hannafin Corporation (doing business as Chomerics North America) such as CHO-SEAL[®] 1285 (Ag-Al in silicone), CHO-SEAL 1212 (Ag-Cu in silicone), and Velostat[™] 1708 from 3M Corporation.

This past work successfully demonstrated the feasibility of using electrical impedance techniques for damage diagnosis, was computationally efficient, and worked well for test articles with simple geometries. The authors' research extends previous work by employing FEM models to achieve greater accuracy for complex models with anisotropic conductivities.⁶ Further extensions include optimizing the network topology to improve efficiency

through a reduction of the number of required computational inputs without compromising the overall fidelity of the damage diagnosis model.

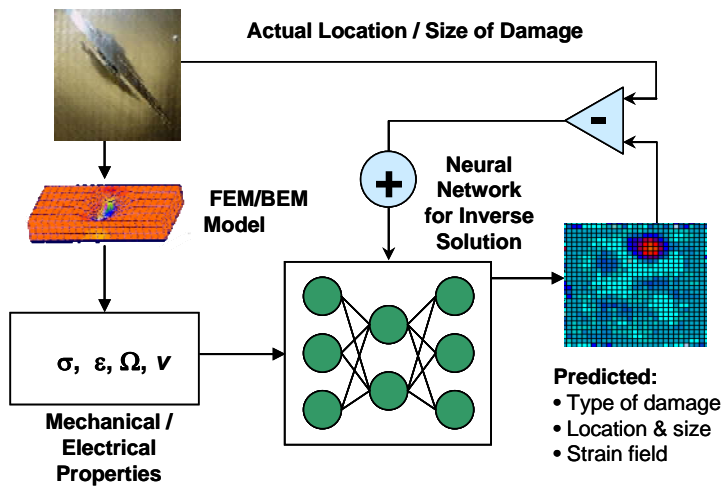


Figure 1. Electrical impedance-based damage diagnosis system.

The authors created FEM models to generate training pattern inputs to the artificial neural network, as shown in the block diagram in Fig. 2. Those blocks to the lower left of the diagonal line represent the ground-based, offline model generation and network training components of the structural health management approach which are not subject to the efficiency constraints of in-flight computational methods. The blocks in the upper right depict the time-critical activities performed in-flight for diagnosis of structural damage in aircraft components.

As shown in the left side of Fig. 2, the FEM models are generated offline as a ground-based learning process and provide the forward solution for the methodology described in this paper. The authors’ approach for diagnosis of structural damage employs a large reference database of possible damage scenarios created from FEM models. Each FEM model is used to derive the forward solution to the damage diagnosis problem by calculating the electrical properties for each damage scenario (that is, compute the electrical properties as a function of the test article configuration including its damage state).

Next, a neural network-based damage diagnosis model is created to solve the inverse problem. Specifically, the goal is to estimate and reconstruct the damage state based on electrical measurements from the test article. This damage diagnosis model is optimized to achieve the best solution by minimizing the error in the estimated damage location and size. Throughout this paper, the term “damage diagnosis model” (DDM) will be used to distinguish the neural network model and diagnosis algorithm from the FEM models.

After the damage diagnosis model has been created and optimized, the resulting model is evaluated using a physical test article to assess the accuracy of the DDM and demonstrate feasibility of the approach. If the DDM is insufficient and does not meet the level of accuracy required by the application, the fidelity of the model is increased through further optimization of the neural network parameters and by increasing the number of damage scenarios.

The activities in each of the ground-based learning blocks shown in Fig. 2 will be discussed further in the following sections; however, the in-flight diagnosis activities are beyond the scope of this paper.

The activities in each of the ground-based learning blocks shown in Fig. 2 will be discussed further in the following sections; however, the in-flight diagnosis activities are beyond the scope of this paper.

Figure 1 conceptually depicts a structural damage diagnosis system based on electrical impedance methods. FEM models are used to estimate the electrical properties of a test article with varying locations and magnitudes of damage. The FEM results are input to a neural network to provide an inverse solution estimating the magnitude and location of damage based on these electrical properties. The differences between the expected and the predicted location and magnitude of the damaged regions are used to train the network to minimize the total error. Once fully trained, the ANN provides an accurate and computationally efficient method for in-flight diagnosis of similar damage states based on sensor measurements of the electrical properties of the vehicle.

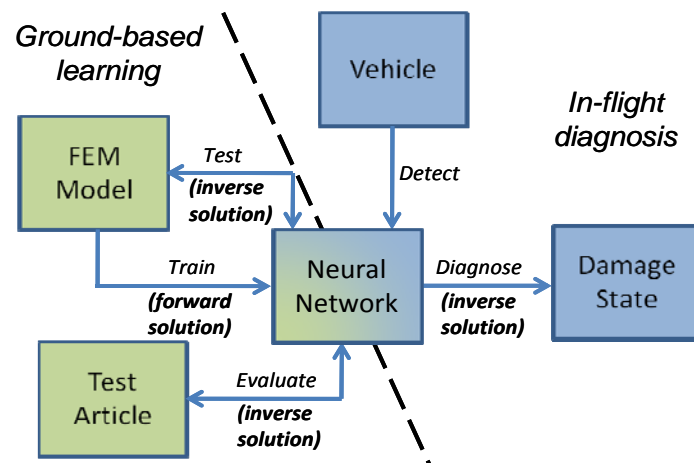


Figure 2. Damage diagnosis methodology.

III. FEM Model – Generating the Forward Solution

For this research effort, the authors modeled an undamaged test article used for experimental evaluation of the models, described later in this paper. While the authors modeled the thermoelectric properties of these test articles, this method could equally be applied to modeling of mechanical properties such as strain.

The test article, an 8" by 8" specimen of CHO-SEAL 1285, is configured with a total of 16 electrodes, as shown in Fig. 3, as both actuators (providing electrical conduction paths for currents injected into the test article) and sensors (measurement test points). Currents are injected using one electrode as the current *source* and another electrode as the current *sink*. A third electrode is used as a voltage ground *reference* for the remaining 13 electrodes employed as voltage *measurement* points.

The combinations of source, sink, and measurement points are varied to reconstruct full field estimates of electrical characteristics from these discrete measurements. The voltages are always measured relative to the fixed reference, with the other 15 available as current source/current sink pairs. The number of current source and sink pairs is given by the number of mathematical combinations of 15 electrodes taken two at a time for a total of $C(15,2) = 105$ combinations. Sampling the voltages at the 13 measurement points for each of the 105 combinations yields a total of 1365 voltages readings, which can be transformed to resistances by applying Ohm's law.

While the electrical properties cannot be modeled directly, an analogy between heat transfer and Ohm's law facilitates the derivation of electrical characteristics from a thermal transfer model. The test article is modeled as a 2D plate as shown in Fig. 3. If a current is applied to a plate, the law of conservation of charge is shown in Eq. (1),

$$\frac{\partial j_x}{\partial x} + \frac{\partial j_y}{\partial y} - f = 0 \quad (1)$$

where f is applied current per unit volume. Ohm's Law of current conduction in the plate gives Eq. (2),

$$j_y = -\sigma_y \frac{\partial V}{\partial y}, j_x = -\sigma_x \frac{\partial V}{\partial x} \quad (2)$$

where V is electric potential; σ is conductivity; j is current density (charge per unit time per unit area) and x, y are the principal material directions. Combining these equations, we obtain the form shown in Eq. (3),

$$-\sigma \left(\frac{\partial^2 V}{\partial x^2} + \frac{\partial^2 V}{\partial y^2} \right) - f = 0 \quad (3)$$

The thermal analog to this equation is the heat transfer relationship shown in Eq. (4),

$$-k \left(\frac{\partial^2 T}{\partial x^2} + \frac{\partial^2 T}{\partial y^2} \right) - q = 0 \quad (4)$$

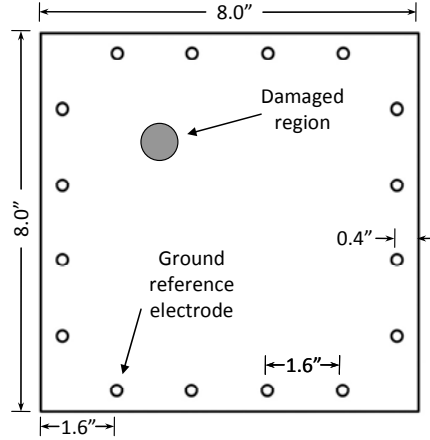


Figure 3. Damaged test article configuration and location of electrodes. Location and size of damage varies with damage scenario.

where T is temperature; k is thermal conductivity; and q is heat flux (applied heat per unit volume). The similarity of Eqs. (3) and (4) allows electrical properties to be derived from heat transfer models,⁷ which are more amenable to FEM modeling methods.

To simplify the analysis, the authors used this thermal analog and conducted a heat transfer analysis in ABAQUS[®] from Dassault Systèmes (Simulia). Current sources and sinks are modeled as heat sources and sinks, the reference voltage ground was modeled as a thermal boundary condition, and voltages are modeled as temperatures. Because of the similarity of the heat transfer and current conduction equations, temperatures modeled in ABAQUS can be readily transformed to voltages using a scaling factor (determined by curve fitting the modeled temperatures to experimentally observed voltages from the test specimen).

First, a FEM model of the undamaged test article is established to provide a baseline from which other models of damage scenarios are derived, each of which includes regions of damage. Next, a Python script generates a series of models of plates with circular holes of random diameter (up to 10% of the plate width) at random locations completely contained within the plate. The models are seeded at eight points around the circumference of each electrode and at 16 points around the damage region. Once seeded, the models are meshed using quadrilateral elements. A parametric study is performed by applying a thermal flux to the 105 combinations of heat source-sink pairs. The script calculates the thermal gradients between the 1365 measurement points and the reference. This analysis is performed on each of the 1000 damage scenarios using different damage sizes and locations.

The damaged regions initially considered were circular holes. More complex forms of damage, such as delamination of composite materials or fatigue cracks in metallics, can also be used. These types of damage were not considered in this effort because the greater complexity of the model and neural network topology result in a significant increase to the computational runtime, which is not practical for this application.

The results of these analyses provide input values for training and testing the neural network. Collectively, the results from these finite element analyses represent the forward solution for estimation of the electrical properties for various damage configurations.

IV. Neural Network – Developing and Training the Inverse Solution

Referring back to Fig. 2, the forward solution described in the preceding section serve as the inputs to an artificial neural network that provides an inverse solution for diagnosis of structural damage. This section of the paper discusses the training of the artificial neural network to develop the DDM as the inverse solution. While the forward solution computes physical parameters (electrical resistance, in this case) from models of damage regions for various locations and sizes, the inverse solution does the opposite – it estimates damage locations and sizes from measured physical parameters such as electrical resistance. Like the generation of the FEM models, the development and training of the neural network is an offline, ground-based process.

Multilayer feed-forward artificial neural networks compute the output values of each node from a linear combination of the inputs to that node and the weights associated with the nodes.⁸ The error associated with the output of the network can be computed as the mean square error of the differences between the actual outputs of the network and the expected outputs used for training. The network is trained by adjusting the weights to minimize the total Mean Squared Error (MSE).⁸ For a single damage scenario, the overall error is reduced by adjusting the individual weights based on the partial derivative of the total error⁹ as shown in Eq. 5,

$$\frac{\partial E_p}{\partial w_{ij}} = \sum_p \frac{\partial E_p}{\partial a_k} \frac{\partial a_k}{\partial w_{ij}} \quad (5)$$

where E_p is the total error for a given pattern (damage scenario), w_{ij} is the weight between hidden node i and input j , and a_k is the weighted sum of the inputs.

For this research effort, the inverse solution was implemented in MATLAB[®] by The MathWorks, Inc.¹⁰ using the Neural Network Toolbox.¹¹ The majority (80%) of the damage scenarios generated by the forward solution are used for training pattern inputs to the neural network and for evaluating and optimizing the network to improve accuracy and computational efficiency. The remaining 20% of the damage scenarios are reserved for testing of the neural network after the network has been fully trained.

As described previously, the test article used was CHO-SEAL 1285, a conductive elastomer consisting of silver-plated aluminum particles in a silicone binder, often used for its electrostatic discharge properties. The test article was 8” by 8” by 0.1”, with a tensile strength of 1.38 MPa and a volume resistivity of 0.008 Ω-cm.

The scatter plot in Fig. 4 shows the residual voltages, or differences between an undamaged test article and the same article with damage, across all measurement conditions. The x axis signifies the 1365 measurement combinations, and the y axis represents the voltage differentials. As can be seen, the sensors detect the differences between the damaged and undamaged states, although the deltas are small (about a 0.1% change or less). Figure 5 shows the same test article, but with the damaged region in a different location from the specimen used in Fig. 4. Table 1 identifies the two damage scenarios used for Figs. 4 and 5.

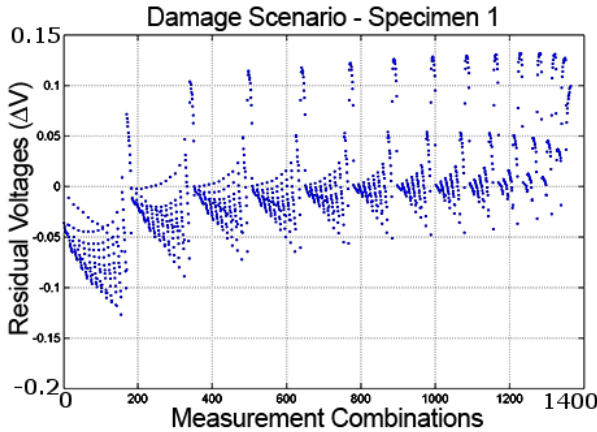


Figure 4. Residual voltages for specimen 1.

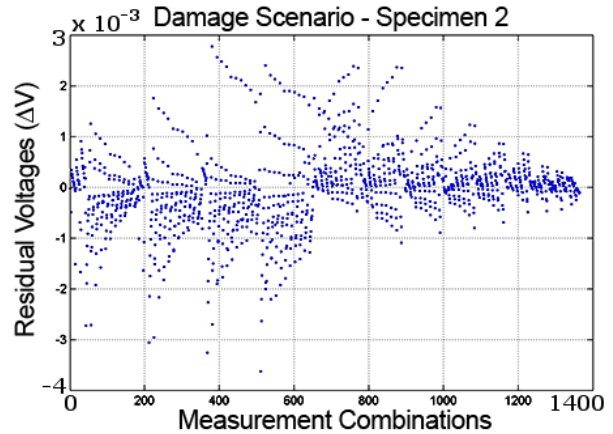


Figure 5. Residual voltages for specimen 2.

A comparison of these two plots clearly shows the residual voltages in Fig. 5 are significantly different from those shown in Fig. 4, signifying that the residual voltages vary with each damage scenario. First, note that the residual voltages in Fig. 5 are nearly two orders of magnitude smaller than those in Fig. 4 (thus requiring a different plot scale). The increased magnitude indicated in Fig. 4 is a result of the larger magnitude of the damage. Second, observe that the shape of the scatter plots is different between the two figures as a result of closer proximity between the damaged region and the reference ground for Specimen 1 than for Specimen 2.

Table 1. Location coordinates and size of damaged regions.

Specimen	Distance from left edge (x)	Distance from bottom edge (y)	Size (radius)
1	1.80"	2.20"	0.73"
2	7.06"	2.86"	0.10"

The presence of structural damage is readily identified by exploiting these differences and can be observed by direct comparison of the residual voltages between the damaged and undamaged specimens. Diagnosis of the location and size, however, is a more challenging problem. To achieve the divergent goals of obtaining the greatest

accuracy in the minimum execution time, the neural network must be tuned to achieve the desired balance between accuracy of damage estimations and computational efficiency. The MATLAB application uses the database of damage scenarios from the forward solution and evaluates them using a range of neural network model topology parameters (such as the choice of computational algorithm, layer sizes, convergence criteria, and learning rate) to obtain an optimal solution to the inverse problem that maximizes accuracy within execution time constraints.

There are many network topology parameters that can be tuned which affect the overall accuracy of the damage estimation model. Underfitting the model with too few hidden layer nodes results in a loss of accuracy due to the inability to find a viable solution, while overfitting with unnecessary hidden nodes can cause the model to “memorize” the patterns used during training but not achieve the correct solution when presented with new data that were not included in the training patterns.

The trained ANN serves as the inverse solution to the problem of diagnosing damage. The goal of an effective neural network approach is to produce the optimum DDM that is adaptive and has the least error while meeting computational time and model size constraints. These criteria are evaluated during the testing and evaluation steps.

V. Testing and Evaluating the Inverse Solution

Previous sections have described the generation of the forward solution (FEM models) and the development of the inverse solution (the DDM). The inverse solution must be tested and, if necessary, updated with additional

damage scenarios to ensure the accuracy goals are achieved by the damage diagnosis model. The neural network is first tested and evaluated against the results of analyses created during the generation of the forward solution, then later evaluated against measurements obtained from a physical test article. These steps, as depicted in Fig. 2, are the last remaining elements of the offline, ground-based learning components.

Since experimental evaluation, even in a laboratory environment, is a time-consuming and expensive process, as much testing as possible is performed using simulated values. The 20% of damage scenarios reserved during the training of the neural network comprise the set of test values used to assess the performance of the neural network. The test values (electrical properties) are provided as inputs to the neural network and the resulting outputs (damage location and size) are compared with the damage location and size used by the FEM model during the generation of the forward solution. The Mean Squared Error (MSE) is computed for all test cases, and the accuracy of the model and computational efficiency is compared with the required level of accuracy and execution time constraints. For this application, a 5% accuracy and 2 second execution time constraint was used. If the DDM produces results outside of either the required accuracy or efficiency levels, adjustments to the neural network configuration, additional training, or both may be required.

Once the model has been tested and meets all requirements using simulated values, the system is ready for experimental evaluation. Until this point, the damage diagnosis model has been trained and tested using parameters estimated by the FEM models. To evaluate the DDM, the authors used an instrumented test article to measure the same electromechanical parameters that were estimated by the FEM models.

These electromechanical properties are measured on both undamaged and damaged test articles, and these data are provided as inputs to the DDM. The estimated location and size of the damage region are compared to the actual location and size of damage present in the test article, and the accuracy of the estimate is computed. The model accuracy is assessed against application-dependent accuracy requirements and execution time constraints, and the model may be further refined if necessary to either increase its accuracy or decrease its execution time.

The experimental evaluation was performed on the test specimen previously described in the FEM modeling section of this paper. The experimental test equipment consists of a Model 2400 Digital SourceMeter, a Model 2750 Digital Multi-Meter/Switch System, and two Model 7709 Matrix Switch Modules, all from Keithley Instruments, Inc. The Model 2400 Digital SourceMeter is a combination current source, voltage source, and single channel multifunction measurement instrument, although it was used solely as a current source for this application. The Model 2750 Digital Multi-Meter/Switch System combines a digital multimeter (DMM) with an expansion chassis for up to five modules for multiplexed data acquisition using standard switch modules. The multimeter supports voltage, current, and resistance measurements, and all of these capabilities were used for evaluating and demonstrating the damage diagnosis model.

To obtain the desired combination of current source, current sink, voltage measurement, and reference ground points, matrix switches were used instead of the multiplexer switches normally used by measurement systems. The Keithley Model 7709 6x8 Matrix Switch Modules consist of 48 double-pole switches, arranged in a matrix of 6 rows by 8 columns. By selectively opening and closing these 48 independently controlled switches, the switch modules allow any arbitrary combination of eight differential test article channels to be connected to six differential instrumentation connections on the Model 2750 digital multimeter. As shown in Fig. 6, these matrix switches can be combined together to expand the number of test article channels.

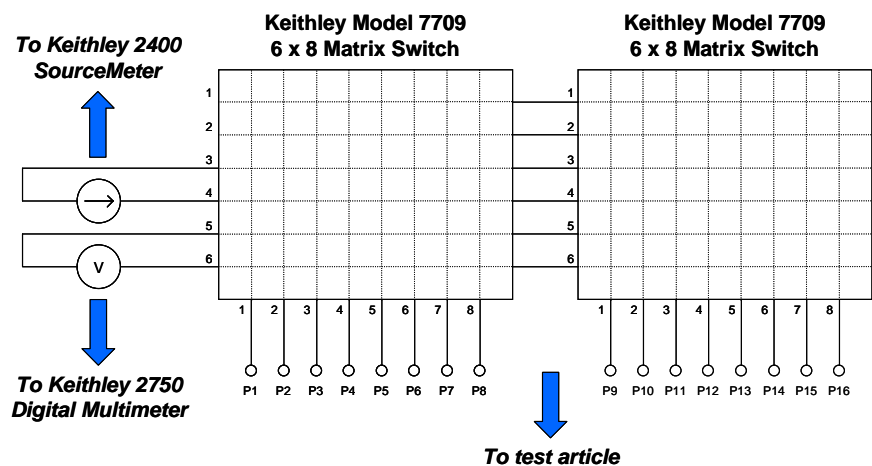


Figure 6. Matrix switch configuration for voltage measurement.

The authors used two of these modules, yielding the equivalent of a 6x16 matrix switch shown in Fig. 6. The 16 columns of the switch are connected to the 16 electrodes connected to the test article. Rows 3 and 4 of the matrix switch provide the excitation from the current source, and rows 5 and 6 are connected to the digital multimeter

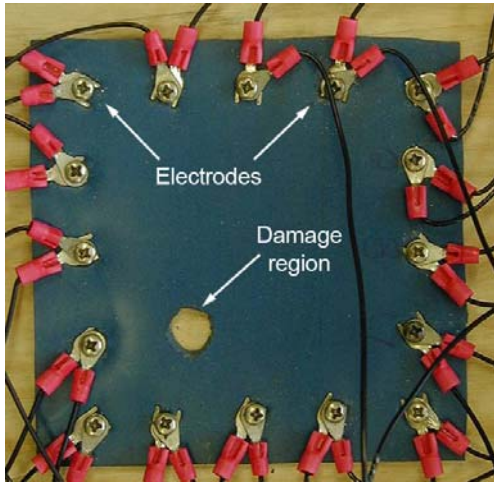
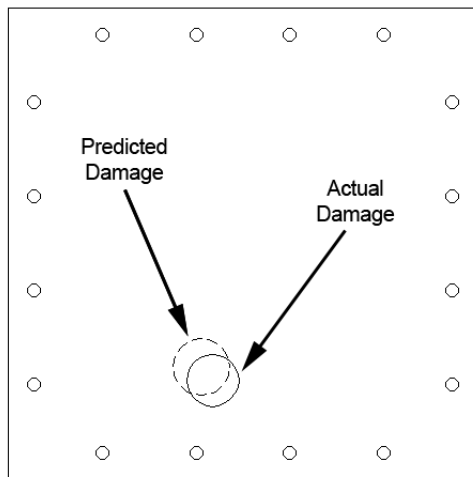


Figure 7. CHO-SEAL 1285 test specimen instrumented for 4-wire resistance measurement.

Both the neural network testing results and the experimental test data were compared with the estimated values from the FEM models to ensure consistency between the computed values and the experimental test results, as discussed in the following section.

VI. Results and Discussion

Preliminary results from testing of the damage diagnosis model show this method to accurately diagnose the location of the damaged region within 2.5 to 4.0 percent and the size of the damage to within 0.5 to 2.0 percent. Figure 8 shows the experimental results, depicting the location and size of the damage predicted by the damage diagnosis model compared with the actual damage for the test article shown Fig. 7.



Predicted: $X = 3.701$, $Y = 2.135$, $R = 0.542$
 Actual: $X = 3.920$, $Y = 1.880$, $R = 0.500$

Figure 8. Comparison of predicted vs. actual location and size of damage.

inputs. For voltage measurements, rows 1 and 2 are not used. However, later evaluation tests use four wire resistance measurements to achieve greater accuracy (by compensating for the internal resistance of the wiring) than the results obtained by applying a current to the test article and measuring the voltages to calculate the resistance. In the four-wire resistance mode, the additional two wires are connected to rows 1 and 2 of the matrix switch module. Figure 7 shows the test article as configured for four-wire resistance measurement.

To evaluate the damage diagnosis model and demonstrate proof of concept, the authors developed an application using LabVIEW[®] from National Instruments Corporation to independently open and close the 96 switches in the matrix modules to control the connection of the current source and the digital multimeter instruments. By closing exactly four of these switches, the current source can be switched to all 105 source-sink combinations. Similarly, the digital voltmeter can be switched to measure the 1365 voltages for each current source and sink combination.

Identifying only the location and size of the damage is most suitable for in-flight estimation of damage; however, a more detailed analysis can be performed if time permits, as shown in Fig. 9. This detailed method divides the specimen into grid-shaped regions, and the likelihood of damage is computed for each grid element. This method provides the most similarity to the Electrical Impedance Tomography method from which it is derived and allows for visual imaging of the material specimen at the expense of computational efficiency. Figure 9 shows the results of the grid method for damage visualization.

These experimental test results in a laboratory environment indicate good correlation between the actual and predicted damage. These results demonstrate a proof of concept of the authors' approach using electrical impedance measurements combined with an artificial network as an effective method for diagnosing structural damage. However, further evaluation is warranted to ensure accurate diagnosis under all conditions. Since not all mathematical functions have unique inverse relationships, inverse solutions may sometimes produce results that are mathematically similar but represent very different damage scenarios, leading to possible misdiagnosis. In such cases, this ambiguity may be resolved by increasing the number of measurements, modifying the neural network configuration, or by varying the location of the sensors.

The authors' damage diagnosis method has been demonstrated to be a successful method for locating and quantifying damage in material specimens using finite element models combined with an artificial neural network. Electrical impedance techniques have been shown to be effective for detecting damage in semiconductive material specimens, and heat transfer models have been demonstrated to be successful for FEM modeling of electrical characteristics. The FEM models work cooperatively with a neural network to provide a complete solution to the problem of diagnosing structural damage, with the FEM models providing a forward solution which is input to an ANN to achieve an inverse solution to the problem of diagnosing structural damage.

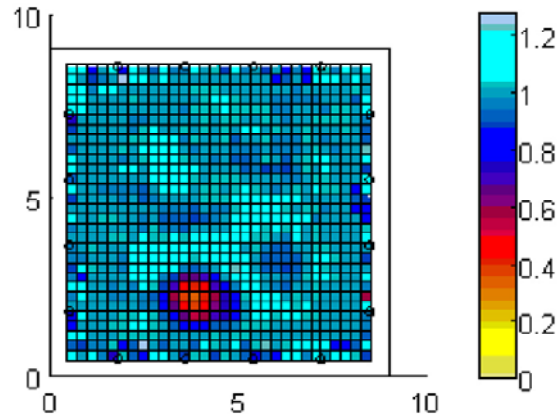


Figure 9. Grid method for damage visualization.

VII. Concluding Remarks

While aviation safety has greatly improved over recent years, there is still a great need for enabling technologies for diagnosis of damage. The damage diagnosis method presented in this paper has been demonstrated to be effective and computationally efficient. These factors, accuracy and efficiency, are both prerequisites for suitability for *in situ*, in-flight diagnosis of structural damage to aircraft components. The damage diagnosis methodology presented in this paper effectively addresses the tradeoff between model accuracy and runtime execution speed.

The creation, optimization, and evaluation of a damage diagnosis model in a controlled laboratory environment is a necessary but not sufficient step towards flight testing using instrumented subcomponents on a sub-scale or full-scale flight test. While achieving this level of technology readiness is beyond the scope of this research effort, a brief mention of the benefits and limitations of flight testing is still warranted. First, subscale or full-scale flight testing provides an assessment of the robustness of the damage diagnosis methods in the presence of both acoustic and electrical noise. Damage diagnosis is challenging under the best of conditions, and in-flight diagnosis is even more challenging.

Second, flight tests afford the opportunity to collect flight data to supplement the simulated values used during the development of the model, increasing the fidelity of the model with no impact on runtime efficiency. One final consideration, however, is that flight testing is expensive and should be performed judiciously.

References

- ¹Guardo, R., Boulay, C., Murray, B., and Bertrand, B., "An Experimental Study in Electrical Impedance Tomography Using Backprojection Reconstruction," *IEEE Transactions on Biomedical Engineering*, Vol. 38, No. 7, 1991, pp. 617-627.
- ²Morabito, F., "Location of Plural Defects in Conductive Plates via Neural Networks," *IEEE Transactions on Magnetics*, Vol. 31, No. 3, 1995, pp. 1765-1768.
- ³Todoroki, A., Tanaka, M., "Delamination Identification of Cross-Ply Graphite/Epoxy Composite Beams Using Electric Resistance Change Method," *Composites Science and Technology*, Vol. 62, 2002, pp. 629-639.
- ⁴Anderson, T. A., Lemoine, G. I., and Ambur, D. R., "An Artificial Neural Network Based Damage Detection Scheme for Electrically Conductive Composite Structures," *44th AIAA/ASME/ASCE/AHS/ASC Structures, Structural Dynamics, and Materials Conference*, AIAA, 2003.
- ⁵Lemoine, G. I., Love, K. W., and Anderson, T. A., "An Electric Potential-Based Structural Health Monitoring Technique Using Neural Networks," *4th International Workshop on Structural Health Monitoring*, September, 2003.
- ⁶Seger, M., Fischer, G., Modre, R., Messnarz, B., Hanser, F., and Tilg, B., "Lead Field Computation for the Electrocardiographic Inverse Problem – Finite Elements versus Boundary Elements," *Computer Methods and Programs in Biomedicine*, Vol. 77, No. 3, 2005, pp. 241-252.
- ⁷Naterer, G. F., *Heat Transfer in Single and Multiphase Systems*, CRC Press, Boca Raton, FL, 2002, p. 36.
- ⁸Hagan, M. T., Demuth, H. B., and Beale, M., *Neural Network Design*, PWS Publishing Company, Boston, MA, 1996, Chaps. 11, 12.
- ⁹Reed, R. D., and Marks II, R. J., *Neural Smthing: Supervised Learning in Feedforward Artificial Neural Networks*, MIT Press, Cambridge, MA, 1999, pp. 49-58.
- ¹⁰MATLAB Ver. R2007b, The MathWorks, Natick, MA, 2007.
- ¹¹Demuth, H., and Beale, M., *Neural Network Toolbox User's Guide*, The MathWorks, Natick, MA, 2000, Chap. 5.